

Computing CNN Loss and Gradients for Pose Estimation with Riemannian Geometry

Benjamin Hou¹, Nina Miolane², Bishesh Khanal^{1,3}, Matthew C.H. Lee^{1,4},
Amir Alansary¹, Steven McDonagh¹, Jo V. Hajnal³, Daniel Rueckert¹,
Ben Glocker¹, and Bernhard Kainz¹

¹Imperial College London, ²INRIA & Stanford, ³Kings College London, ⁴HeartFlow

Abstract. Pose estimation, *i.e.* predicting a 3D rigid transformation with respect to a fixed co-ordinate frame in, $SE(3)$, is an omnipresent problem in medical image analysis with applications such as: image rigid registration, anatomical standard plane detection, tracking and device/camera pose estimation. Deep learning methods often parameterise a pose with a representation that separates rotation and translation. As commonly available frameworks do not provide means to calculate loss on a manifold, regression is usually performed using the L2-norm independently on the rotation's and the translation's parameterisations, which is a metric for linear spaces that does not take into account the Lie group structure of $SE(3)$.

In this paper, we propose a general Riemannian formulation of the pose estimation problem. We propose to train the CNN directly on $SE(3)$ equipped with a left-invariant Riemannian metric, coupling the prediction of the translation and rotation defining the pose. At each training step, the ground truth and predicted pose are elements of the manifold, where the loss is calculated as the Riemannian geodesic distance. We then compute the optimisation direction by back-propagating the gradient with respect to the predicted pose on the tangent space of the manifold $SE(3)$ and update the network weights. We thoroughly evaluate the effectiveness of our loss function by comparing its performance with popular and most commonly used existing methods, on tasks such as image-based localisation and intensity-based 2D/3D registration. We also show that hyper-parameters, used in our loss function to weight the contribution between rotations and translations, can be intrinsically calculated from the dataset to achieve greater performance margins.

1 Introduction

Intensity-based registration and landmark matching are the de facto standards to align data from multiple image sources into a common co-ordinate system. Applications that require intensity-based registration include *e.g.*, atlas-based segmentation [1], motion-compensation [16], tracking [11], or clinical analysis of the data visualised in a standard co-ordinate system. These often require manual initialisation of the alignment since general optimisation methods often cannot find a global minimum from any given starting position on the cost function.

An initial rigid registration can be achieved by selecting common landmarks [2] through an iterative agent, which impedes hard real-time constraints or less robustly through local image descriptors [20].

Convolutional neural networks (CNNs) have shown promising results for intra and inter modal alignment [11,5]. The general idea for these approaches is that information about a learn-able canonical co-ordinate system is encoded directly in the features of an image. Early work in this domain showed that image’s pose (i.e. position and orientation) can be regressed relatively to a canonical alignment from a large set of training images sampling the canonical space [8]. Follow-up formulations for medical applications showed similar success for motion compensation and device localisation [11,5]. However, these approaches rely on heuristic approximations and manual fine-tuning of the CNN loss used to characterise the prediction error on the pose. This fosters domain shift problems and limits options for interchangeable application of various deep learning pose estimation models.

Contribution: To solve this problem, we introduce a new loss function that calculates the geodesic distance of two poses on the $SE(3)$ manifold, from a data-adaptive Riemannian metric. We derive appropriate gradients that are required for CNN back propagation. Our method couples the translation and rotation parameters, and regresses them simultaneously as one parameter on the Lie algebra $\mathfrak{se}(3)$. We show that our loss function is agnostic to the architecture by training different CNNs and can effectively predict poses that are comparable to state-of-the-art methods. In addition, we demonstrate that hyper-parameters tuning for our loss function can be directly calculated from the dataset, thus avoiding long and expensive optimisation searches to boost performance. Finally, we validate quantitatively by benchmarking the performance of our loss function with current state-of-the-art methods, and validate their statistical significance with Student’s t-test.

Background: A pose, i.e. a rigid transformation in 3D, is an element of the Lie group $SE(3)$, the Special Euclidean group in 3D. A pose has two components; a rotation component of group $SO(3)$ and a translation component of \mathbb{R}^3 . $SE(3)$ has the following convenient matrix representation (called the homogeneous representation):

$$SE(3) = \left\{ X \mid X = \begin{bmatrix} R & t \\ 0 & 1 \end{bmatrix}, t \in \mathbb{R}^3, R \in SO(3) \right\} \quad (1)$$

In usual implementations of $SE(3)$, the rotation matrix R can be parameterised in any form as long as the matrix structure is implicitly imposed. R can be stored as Euler angles, quaternions, axis-angle or $SO(3)$ rotation matrix. This needs to be considered carefully, especially when designing deep learning applications, as the numerical properties of each parameterisation can hamper efficacy.

Euler angles parameterisation is undesirable as it suffers from Gimbal lock [3], where a degree of freedom is lost when two rotation axis becomes aligned. Furthermore, Hyunh et al. [6] has shown that the parameterisation is not unique,

as two different mappings can represent the same rotation. Matrix parameterisation carries 9 parameters, it is over parameterised therefore making it undesirable. Also, orthonormality of the rotation matrix must be preserved, as a non-orthogonal rotation matrix can result in skewed or sheared transformations. Quaternion parameterisation are often favoured as it can be mapped to valid transformations after normalisation.

However, the parameterisation chosen for the rotation is almost never coupled with the parameterisation of the translation, thus denying the intrinsic structure of $SE(3) = SO(3) \times \mathbb{R}^3$. Here, we choose to represent the rotation and the translation together as an element of the Lie algebra of $SE(3)$, i.e. its tangent space at the identity element of the group, denoted $\mathfrak{se}(3)$. It represents the best linear approximation of $SE(3)$ around its identity element. Since the Lie group $SE(3)$ is 6-dimensional, an element of $\mathfrak{se}(3)$ is a 6D vector.

One can define a collection of distances on $SE(3)$, which can be used as loss functions in deep learning applications. A popular choice for the loss is the Euclidean distance associated to the L2-norm. However, the L2-norm is not desirable on $SE(3)$ since it does not respect the manifold’s non-linearity and can lead to unpredictable behaviours. It is also undesirable to use two separate L2-norms on $SO(3)$ and \mathbb{R}^3 since $SE(3)$ is not a direct product, and $SO(3)$ itself is non-linear: this can be observed visually with quaternions, e.g., the Euclidean distance of two quaternions can be small, despite the rotation being large. This disparity, between the loss and the target, causes network weight updates to be sub optimal, hence it is desirable to have a loss function that respects the structure of $SE(3)$.

Related Work: Popular deep learning frameworks available today, such as Caffe, TensorFlow, Theano, PyTorch, do not provide the means to regress on $SE(3)$, as the common losses used are cross-entropy for probabilities or a p-norms for distances.

Kendal et al. [8] uses the L2-norm to regress parameters on the Lie algebra $\mathfrak{se}(3)$ directly, with a β parameter to weight the contribution between rotation and translation. This was similarly performed by authors in [14,18,11,10], who use the predicted parameters for registration tasks. Alternatively, [9,17] re-parameterised the pose parameters as projected co-ordinates on a 2D view plane. This was similarly performed by [5,4] with Anchor Points, where three arbitrary selected reference points on a 2D plane define the plane’s location in 3D space. Using the L2-norm to calculate the Euclidean distance between a predicted projection co-ordinate and the ground truth projection co-ordinate is appropriate, as the L2-norm is the appropriate metric. To the best of our knowledge, there is currently no loss function that respects the full Lie group structure of $SE(3)$, for example invariant Riemannian metrics on $SE(3)$ have not been used.

2 Method

The core of our method is to implement a new loss layer: we define the loss as the geodesic distance on $SE(3)$ equipped with a left-invariant Riemannian metric,

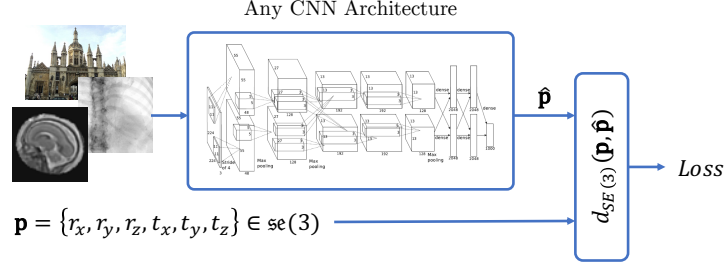


Fig. 1. CNN architecture using a Riemannian geodesic distance as the loss on $SE(3)$.

Figure 1. Then, the overall network structure is agnostic to PoseNet’s neural network architecture.

Left-invariant Riemannian metric on $SE(3)$: A Riemannian metric on $SE(3)$ is a smooth collection of positive definite inner products on each tangent space of $SE(3)$. Then, $SE(3)$ becomes a Riemannian manifold. With a left-invariant metric, it is enough to define an inner product on the tangent space at the identity of $SE(3)$, and then “propagate” it: the metric is s.t. $\forall u, v \in T_{p_1}SE(3)$ and $\forall p_1, p_2 \in SE(3)$: $\langle DL_{p_1}(p_2)u, DL_{p_1}(p_2)v \rangle |_{L_{p_1}p_2} = \langle u, v \rangle |_{p_2}$ where L_{p_1} is the left translation by p_1 : $L_{p_1}(p_2) = p_1 \circ p_2$, and $DL_{p_1}(p_2)$ its differential at p_2 . Defining an inner product Z at $p_2 = \text{identity}$ enables us to get a metric Z_{p_1} at the tangent space of any pose p_1 of $SE(3)$ [13], and thus to compute inner products and norms of tangent vectors at p_1 .

Loss and gradient: We use the loss function: $\text{loss}(\mathbf{p}, \hat{\mathbf{p}}) = \text{dist}_{SE(3)}^Z(\mathbf{p}, \hat{\mathbf{p}})^2 = \|\text{Log}_{\hat{\mathbf{p}}}^Z(\mathbf{p})\|_{Z_{\hat{\mathbf{p}}}}^2$ where $\text{dist}_{SE(3)}^Z$ is the geodesic distance and Log is the Riemannian logarithm at $\hat{\mathbf{p}}$ i.e. a tangent vector at $\hat{\mathbf{p}}$. We use a left-invariant Riemannian metric, thus: $\text{loss}(\mathbf{p}, \hat{\mathbf{p}}) = \|DL_{\hat{\mathbf{p}}^{-1}}.\text{Log}_{\hat{\mathbf{p}}}^Z(\mathbf{p})\|_Z^2$, where we now have a tangent vector at the identity and we can use the inner product Z . If we take Z being the canonical inner product at identity, this is the L2-norm but on the tangent vector transported from $\hat{\mathbf{p}}$ to identity using the differential $DL_{\hat{\mathbf{p}}^{-1}}$. The backward gradient corresponding to the loss seen as a function of $\hat{\mathbf{p}}$ is $\nabla_{\hat{\mathbf{p}}}\text{loss}(\mathbf{p}, \hat{\mathbf{p}}) = -2 \cdot \text{Log}_{\hat{\mathbf{p}}}^Z(\mathbf{p})$ [15] which is a tangent vector at $\hat{\mathbf{p}}$.

Implementation: The inputs to the loss layer are the poses \mathbf{p} and $\hat{\mathbf{p}}$ for ground truth and prediction respectively. We represent a pose with `geomstats` implementation [12] i.e. as the Riemannian Logarithm of canonical left-invariant metric on $SE(3)$ s.t. $p = \{r, t\} = \{r_x, r_y, r_z, t_x, t_y, t_z\} \in \mathbb{R}^6$. With this parameterisation, the rotation r is in axis-angle parameterisation, the inner product Z is a 6x6 positive definite matrix and the differential $DL_{\hat{p}}$ of the left translation is the 6x6 jacobian matrix: $J_{\hat{p}} = \begin{pmatrix} \frac{\partial L_{\hat{p}}^r}{\partial r} & \frac{\partial L_{\hat{p}}^r}{\partial t} \\ \frac{\partial L_{\hat{p}}^t}{\partial r} & \frac{\partial L_{\hat{p}}^t}{\partial t} \end{pmatrix}$. We denote $v_t = \text{Log}_{\hat{\mathbf{p}}}^Z(\mathbf{p})$

which is a tangent vector at $\hat{\mathbf{p}}$ in this parameterisation. The loss is calculated by $\text{loss}(\mathbf{p}, \hat{\mathbf{p}}) = v_t^T * J_{\hat{\mathbf{p}}^{-1}}^T * Z * J_{\hat{\mathbf{p}}^{-1}} * v_t$ where $*$ is the matrix multiplication and the Riemannian logarithm v_t is given by `geomstats`. The gradient is calculated

by: $\nabla_{\hat{\mathbf{p}}}\text{loss}(\mathbf{p}, \hat{\mathbf{p}}) = -2 * J_{\hat{\mathbf{p}}^{-1}}^T * Z * J_{\hat{\mathbf{p}}^{-1}} * v_t$. By the time of the conference, we will provide the source code of our implementation on github.

3 Experiments and Results

We evaluate our novel loss function on three datasets: **(Exp1)** the publicly available PoseNet dataset [8], which allows a direct comparison to state-of-the-art in Computer Vision, and further evaluate optimisation strategies for these experiments. **(Exp2)** the common C-Arm X-Ray to Computed Tomography (CT) alignment problem with data from [5]. Furthermore, in **(Exp3)**, the pose estimation dataset for motion compensation in fetal Magnetic Resonance Imaging (MRI) from [4].

In each experiment, we benchmark existing $SE(3)$ parameterisation strategies with the respective loss function used. PoseNet: direct regression of parameters on the Lie algebra $\mathfrak{se}(3)$, where a combination of quaternion and translation parameters are regressed using L2-norms with a static β parameter to weight the respective contribution. Anchor Points formulation: a re-parameterisation of $SE(3)$ in Euclidean space, where three statically defined points in 3D space defines a plane. Each Anchor Point is regressed independently using the L2-norm. Finally, our $SE(3)$ loss function, i.e., the geodesic distance on the Riemannian manifold.

All experiments are conducted using the Caffe framework, on a computer equipped with an Intel i7 6700K CPU and Nvidia Titan X Pascal GPU.

Exp.1: Metric Localisation on Natural Images: In this experiment, we replicated PoseNet’s original experiment [8] on the King’s College dataset as a baseline benchmark. [8] extracted images from a series of videos, and fed them into a structure from motion pipeline to create a 3D model in order to extract plane locations with respect to a world co-ordinate reference frame. The parameterisation of this dataset are quaternions with translation offsets. We mirrored the dataset using axis-angle representation instead of quaternions, and used our $SE(3)$ loss function as regressor. Both networks were trained with a GoogLeNet [19] base architecture with no parameter weighting. Table 1 summarises the results.

Table 1. Mean Error of Loss Functions on Natural Images w/o Parameter Weights

	R_x	R_y	R_z	t_x	t_y	t_z	G.D.
PoseNet	4.141	7.774	4.597	1.341	1.139	0.154	23.629
$SE(3)$	4.306	6.675	11.580	1.307	1.149	0.155	14.973

We convert the predicted and ground truth pose to Euler angles in degrees and translation in meters, along with the geodesic distance (G.D.) on the manifold. Table 1 shows the average errors of each parameter. It can be seen that

the error is similar in each Euler and translation parameters, which is confirmed by Student’s t-test. However, the geodesic distance error of $SE(3)$ is much lower compared to PoseNet. Despite this, computing Student’s t-test still shows no significant difference, which is caused by the large variance of PoseNet.

To tune the weight parameter β , Kendall et al. [8] performed grid search and found that $\beta = [120, 750]$ works best for indoor scenes and $\beta = [250, 2000]$ for outdoor scenes. Grid search is computationally very expensive, and it can be difficult to find an optimal value if the search interval is coarse. We show here that we can compute a data-adaptive Riemannian metric on $SE(3)$ to weight the contribution of each parameter in the loss.

We first train the network with no weightings, followed by an inference pass through the entire validation dataset. We compute the prediction error as the rigid transformation: $(y_{true})^{-1} \circ y_{pred}$ and consider the dataset of their Riemannian logarithms at the identity $\{X_i\}_i$. The parameter weightings are then calculated by $\text{diag}(\text{cov}(X_i)^{-1})$. The diagonal of the covariance matrix shows the variance of each parameter, whereas the inverse shows how tightly coupled it is to the mean. Thus, the higher the diagonal element, the tighter the variable is clustered. Elements, that are more sparsely coupled, are weighted less as they are likely to induce errors. The optimal weightings for the King’s College dataset from [8] are: $\text{diag}(\text{cov}(X_i)^{-1}) = \{0.147, 0.954, 0.261, 0.001, 0.003, 0.002\}$.

Table 2 shows the performance of the networks retrained with suggested weightings. Benchmarking with Geodesic Distances is not performed here, as it is not possible to map hyper-parameters across different metrics.

Table 2. Mean Error of Loss Functions on Natural Images w/ Parameter Weights

	R_x	R_y	R_z	t_x	t_y	t_z	G.D.
PoseNet	1.790	2.612	2.371	1.161	1.306	0.154	—
$SE(3)$	1.870	3.143	3.662	1.759	1.240	0.156	—

The newly trained networks shows significantly improved performance compared to the networks trained without parameter weighting. However Student’s T-test still shows no significant difference between errors induced by PoseNet and $SE(3)$.

Exp.2: Plane Detection on C-ARM Imaging: [5] demonstrated the versatility of CNNs for performing 2D/3D registration of C-Arm X-ray images to CT volumes using Anchor Points. In this experiment, we replicate the 2D/3D registration task and evaluate the performance with the newly proposed $SE(3)$ parameterisation and loss regressor. For comparison, a network was also trained with PoseNet’s parameterisation. All weight parameters are set to a default of 1. Table 3 shows the performance of each parameterisation. CaffeNet is used as base CNN architecture.

Here, we convert the predicted and ground truth poses to Euler angles in degrees, and translation to millimeters. Similar to Exp1, the average error for

Table 3. Mean Error of Loss Functions on DRR (Digitally Reconstructed Radiographs)

	R_x	R_y	R_z	t_x	t_y	t_z	G.D.
PoseNet	7.960	3.136	7.547	62.650	57.315	45.852	15201.845
Anchor Points	7.274	2.511	7.059	59.292	54.889	40.576	15115.858
$SE(3)$	8.243	3.697	7.924	58.647	55.477	44.189	14170.722*
Healthy Patient Dataset							
	R_x	R_y	R_z	t_x	t_y	t_z	G.D.
PoseNet	10.653	5.788	10.760	69.107	72.238	57.726	23495.708
Anchor Points	8.540	4.060	8.553	65.521	68.543	54.133	21725.921
$SE(3)$	10.511	6.789	11.913	62.588	68.747	54.110	19624.246*
Pathological Patient Dataset							

Euler parameters and translation parameters (for both healthy and pathological patients) are similar, and insignificant as confirmed by Student’s t-test. However, there is a noticeable trend in average geodesic distance errors. Student’s t-test showed significant difference (marked by *) between $SE(3)$ loss compared to PoseNet and Anchor Points for both datasets. This shows that the geodesic metric is able to quantify properties that the metric expressed in Euler-translation parameters cannot.

Exp.3: 2D/3D Registration on fetal brain MRI: We replicate the results evaluation method from [4], and evaluated our loss regressor for 2D/3D registration used during motion compensation of fetal MRI data in canonical organ space. [4] uses aligned, reconstructed 3D brain volumes to learn a canonical orientation space and utilises an approach based on GoogLeNet to reorient unseen 2D brain slices into their correct anatomical location in this space. To sample the canonical training space we use the same Euler iteration method (*i.e.*, 18° steps in R_x R_y R_z between -90° and $+90^\circ$, and 2mm offsets in T_z constrained between -40 and 40) to generate 1.12M images for the training set. The evaluation method is performed similarly as [4], with the performance summarised in Table 4. The validation dataset is composed of brain slices sampled with random Euler angles between -90° and $+90^\circ$, and random offsets between -40 and +40.

Table 4. Mean Error of Loss Functions on Fetal Brain Images

	CC	MSE	PSNR	SSIM	G.D.
PoseNet	0.8199	1046.4	18.6509	0.5448	18.1708
Anchor Points	0.8378	935.0	19.3564	0.5845	15.7504
$SE(3)$	0.8732*	724.9713*	20.7484*	0.6470*	10.0836*

Our $SE(3)$ loss function shows drastic improvement in all image similarity metrics (Cross Correlation, Mean Squared Error, Peak Signal-to-Noise Ratio and

Structural SIMilarity). This is confirmed by Student’s t-test which shows significant difference. This is crucial for Slice-to-Volume applications as the metric for slice alignment is derived from the metrics used above [7].

Discussion: A pose is a combination of rotation and translation, therefore it seems reasonable that a CNN predicting a pose should use a metric that accounts for both of them simultaneously. However, one should compare metrics with a target application. Metrics are perceptually a method of measurement with its own set of rules, *e.g.*, imperial vs. metric system for quantifying distances. Choosing a metric for a target application is not always straight forward and often a question of required precision, *e.g.*, one would not measure the diameter of a pinhead with a meter rule, nor measure distance between cities with a caliper. We have shown that our loss function, using a Riemannian geodesic distance on $SE(3)$ is better suited for medical registration tasks as shown in Exp2 and Exp3. Exp2 shows each test case yielding no significant difference on Euler and translation parameters, with significant difference on geodesic parameters. This suggests that Euler-translation parameters separately are not able to fully quantify the properties of $SE(3)$. In Exp3, our loss function was able to significantly improve the image similarity metrics, as used by Slice-to-Volume motion compensation algorithms.

4 Conclusion

In this work, we have presented a novel loss function to regress poses on the Lie group $SE(3)$, and derive the necessary gradients required for CNN training. We show that our method alleviates the need of re-parameterising regression parameters, which addressed the domain shift problem of deep learning applications. Our approach achieves similar results to manually fine-tuned approximations out-of-the-box, *e.g.*, for data from a new scanner. This is demonstrated on the current state-of-the-art for pose estimation, PoseNet, where we show that our method achieves similar performance as the carefully tuned approximation used in [8]. We also show significant improvements for medical image pose estimation and outperform the state-of-the-art in this domain [5,4].

References

1. Aljabar, P., et al.: Multi-atlas based segmentation of brain images: Atlas selection and its effect on accuracy. *NeuroImage* 46(3), 726 – 738 (2009)
2. Ghesu, F.C., et al.: An Artificial Agent for Anatomical Landmark Detection in Medical Images. In: *MICCAI’16, Part III*. pp. 229–237 (2016)
3. Hemingway, E.G., et al.: Perspectives on euler angle singularities, gimbal lock, and the orthogonality of applied forces and applied moments. U.C. Berkeley (2017)
4. Hou, B., et al.: 3D Reconstruction in Canonical Co-ordinate Space from Arbitrarily Oriented 2D Images. *IEEE Trans. Med. Imaging* PP(99), 1–1 (2018)
5. Hou, B., et al.: Predicting slice-to-volume transformation inpresence of arbitrary subject motion. In: *MICCAI’17*. pp. 296–304 (2017)

6. Huynh, D.Q.: Metrics for 3d rotations: Comparison and analysis. *Journal of Mathematical Imaging and Vision* 35(2), 155–164 (2009)
7. Kainz, B., et al.: Fast Volume Reconstruction from Motion Corrupted Stacks of 2D Slices. *IEEE Trans. Med. Imag.* 34(9), 1901–13 (2015)
8. Kendall, A., et al.: PoseNet: A convolutional network for real-time 6-DOF camera relocalization. In: *ICCV*. pp. 2938–2946 (2015)
9. Kendall, A., Cipolla, R.: Geometric loss functions for camera pose regression with deep learning. In: *Proceedings of the IEEE CVPR* (2017)
10. Liao, R., et al.: An artificial agent for robust image registration. In: *AAAI*. pp. 4168–4175 (2017)
11. Miao, S., et al.: A CNN Regression Approach for Real-Time 2D/3D Registration. *IEEE Trans. Med. Imag.* 35(5), 1352–1363 (2016)
12. Miolane, N.: *Geomstats: Computations and statistics on manifolds with geometric structures*. (Feb 2018), <https://github.com/ninamiolane/geomstats>
13. Miolane, N., Pennec, X.: Computing Bi-Invariant Pseudo-Metrics on Lie Groups for Consistent Statistics. *Entropy* 17(4), 1850–1881 (Apr 2015)
14. Pei, Y., et al.: Non-rigid craniofacial 2d-3d registration using cnn-based regression. In: *Deep Learning in Medical Image Analysis and Multimodal Learning for Clinical Decision Support*, pp. 117–125. Springer (2017)
15. Pennec, X.: Probabilities and statistics on riemannian manifolds: Basic tools for geometric measurements. In: *NSIP*. pp. 194–198. Citeseer (1999)
16. Rousseau, F., et al.: Registration-Based Approach for Reconstruction of High-Resolution In Utero Fetal MR Brain Images. *Acad Radiol* 13(9), 1072–1081 (2006)
17. Sarkis, M., Diepold, K.: Camera-pose estimation via projective newton optimization on the manifold. *IEEE Trans. Image Process.* 21(4), 1729–1741 (Apr 2012)
18. Sloan, J., et al.: Learning rigid image registration - utilizing cnns for medical image registration (2018), <http://eprints.gla.ac.uk/156798/>
19. Szegedy, C., et al.: Going deeper with convolutions. In: *IEEE CVPR'15* (2015)
20. Zitov, B., Flusser, J.: Image registration methods: a survey. *Image and Vision Computing* 21(11), 977 – 1000 (2003)